Biochemical Society Transactions (2021) **49** 2627–2638
https://doi.org/10.1042/BST20210444

Review Article

Applications of Cryo-EM in small molecule and biologics drug design

Joshua A. Lees, Joao M. Dias and Seungil Han

Discovery Sciences, Medicine Design, Pfizer Worldwide Research and Development, Groton, CT 06340, U.S.A.

Correspondence: Seungil Han (seungil.han@pfizer.com)

Electron cryo-microscopy (cryo-EM) is a powerful technique for the structural characterization of biological macromolecules, enabling high-resolution analysis of targets once inaccessible to structural interrogation. In recent years, pharmaceutical companies have begun to utilize cryo-EM for structure-based drug design. Structural analysis of integral membrane proteins, which comprise a large proportion of druggable targets and pose particular challenges for X-ray crystallography, by cryo-EM has enabled insights into important drug target families such as G protein-coupled receptors (GPCRs), ion channels, and solute carrier (SLCs) proteins. Structural characterization of biologics, such as vaccines, viral vectors, and gene therapy agents, has also become significantly more tractable. As a result, cryo-EM has begun to make major impacts in bringing critical therapeutics to market. In this review, we discuss recent instructive examples of impacts from cryo-EM in therapeutics design, focusing largely on its implementation at Pfizer. We also discuss the opportunities afforded by emerging technological advances in cryo-EM, and the prospects for future development of the technique.

Introduction

Structure-based drug design (SBDD) has been an essential tool in pharmaceutical development for decades. Structures of macromolecular drug targets, especially when bound to modulators, can reveal ligand-binding pockets and pinpoint protein–ligand interactions that influence the mechanism of action, potency, and specificity. Used iteratively and synergistically with biochemistry, pharmacology, and input from medicinal and computational chemists, SBDD is a powerful tool for optimizing drug efficacy and safety. Its ability to speed and inform compound screening and design has helped to bring many first-in-class drugs to market. While X-ray crystallography was long the cornerstone of SBDD, the rise of cryo-electron microscopy (cryo-EM) in recent years, driven by advances in sample preparation, imaging, and data processing technologies, has changed the landscape of SBDD and structural biology more broadly. Between 2010 and 2020, the proportion of PDB depositions solved by EM grew from 0.7% to 17%, with nearly 50% of reported cryo-EM structures in 2020 solved at resolutions of 3.5 Å or better [1], and of these, 72% were solved with a small-molecule ligand. Cryo-EM, which bypasses crystallization and requires relatively small quantities of protein, has begun to make impacts in structure-based therapeutics design across multiple modalities [2].

While pharmaceuticals target a broad range of protein families, integral membrane proteins constitute some of the largest and most important, by some estimates already comprising over 60% of known small-molecule drug targets [3,4]. Cryo-EM has been particularly enabling of SBDD for these targets, partly because they have often proved challenging to crystallize. For this reason, we have devoted much of this review to three of the largest classes of druggable membrane proteins: G protein-coupled receptors (GPCRs), ion channels, and solute carriers (SLCs).

Received: 13 September 2021
Revised: 22 October 2021
Accepted: 27 October 2021

Version of Record published: 23 November 2021

Biochemical Society Transactions (2021) **49** 2627–2638
https://doi.org/10.1042/BST20210444

GPCRs form the largest class of druggable membrane protein targets, with ∼800 members in humans. GPCRs are targeted by 30–50% of all currently marketed small-molecule drugs [5,6], but nearly 100 remain 'orphaned', with their biological ligands unidentified. Cryo-EM has enabled over 150 novel GPCR structures in the last 5 years [7], a seismic shift in our ability to target these proteins with therapeutics.

Ion channels, comprising over 400 known genes in humans, are targeted by 15–20% of all current drugs [6,8], modulating homeostatic mechanisms linked to ion balance, blood pressure, and cell division. They are also important neuromodulators, with consequences for cognition, sensation, and motor control. Structural analysis of ion channels is particularly critical for reducing off-target effects.

An emerging target family, SLC proteins comprise over 400 members in 66 families [9,10], widely distributed among tissues and cell types, which regulate ion gradient-driven uptake of metabolites including amino acids, sugars, lipids, nucleotides, and others. SLCs are linked to a variety of human disorders, including cancer [11], and over 100 single-gene diseases are linked to SLC defects, giving them enormous potential as therapeutic targets [12].

Large molecular assemblies, such as viruses and ribosomes [13–16], were some of the earliest success stories for cryo-EM. As pharmaceutical companies develop vaccines and biologics, cryo-EM has revealed the structural details underlying vaccine efficacy and informing design. This work is still highly relevant, particularly in the face of emerging infectious threats, such as SARS-CoV-2.

In this review, we discuss recent structural analyses of selected targets by cryo-EM at Pfizer and elsewhere and how this powerful tool can be used to inform therapeutics design. We also discuss the current technological landscape and exciting opportunities for drug design from emerging technologies that will revolutionize our use of cryo-EM in the coming years.

GPCRs

GPCR structures have been enabled by cryo-EM at an increasing rate in recent years. While class A GPCRs form the bulk of novel structures, other receptor classes, including B1, B2, C, D1, and F, are beginning to appear in structural databases. Most have been enabled in the active state with agonist peptides, small molecules or positive allosteric modulators (PAMs) by forming complexes with β-arrestin or heterotrimeric G-proteins stabilized by auxiliary antibodies or nanobodies (for example: Nb35 and ScFv16) [17,18]. In the active state, protrusion of the G protein complex from the transmembrane region facilitates particle identification and alignment from cryo-EM datasets, enabling high-resolution structures. A growing toolbox, including truncated (miniG) [19], dominant negative [20], and chimeric [17] forms of the G protein alpha subunit, as well as GPCR-cytochrome b_{562}RIL (BRIL) fusions with associated Fab fragments [21], has simplified the process of solving agonist-bound GPCR structures. While a growing number of unliganded GPCR structures are now emerging, only a few have been determined with antagonist small molecules, with prominent examples in GPCR family C being the γ-aminobutyric acid type B ($GABA_B$) receptor subunit 1 with the inverse agonist CGP-55845 [22], $GABA_B$ receptor subunit 2 with antagonist CGP-54626 [23,24], the metabotropic glutamate receptor mGluR2 with antagonist LY341495 [25], and the calcium-sensing receptor with the NAM NPS-2143 [26,27]. In these examples, the absence of the G protein makes structural solution challenging, but receptor dimerization in family C GPCRs, as well as the large receptors' extracellular domains, provided enough protein mass to support reconstruction.

Glucagon-like peptide 1 receptor (GLP-1R) offers an instructive example of the use of cryo-EM to understand the pharmacology of GPCRs for drug discovery. Targeted for the treatment of type 2 diabetes and obesity, GLP1-R is a class B1 GPCR found in pancreatic β-cells, with a role in the regulation of insulin secretion. The structure of rabbit GLP-1R with heterotrimeric Gs-protein was initially determined by cryo-EM in the presence of the GLP-1 peptide [28], followed by its human ortholog in the presence of exendin-P5 [29]. In 2020, cryo-EM was used to characterize the mode of action of an agonist compound, PF-06883365 [30]. The structure of GLP-1R bound to PF-06883365 revealed a mechanistically critical tryptophan residue (W33) unique to primates. Rotation of the GLP-1R extracellular domain shifts W33 to close the ligand-binding pocket by forming hydrophobic interactions with PF-06883365. This phenomenon explains the compound's reduced potency in other mammals, where serine occurs in the equivalent position, and was confirmed by mutational analysis. The structure also offered structure–activity relationship (SAR) insights for this compound series by explaining a potency gain from the introduction of a 6-carboxylic acid motif to the compound's benzimidazole region, which creates productive interactions with R380. Recently published cryo-EM structures, from the

Monash Institute of Pharmaceutical Sciences, of GLP-1R complex bound to Pfizer clinical candidate PF-06882961 and CHU-128 [31] (Figure 1A), confirmed this agonist series' binding mode and the role of W33 in species selectivity, providing important knowledge needed for pre-clinical screening of compounds in non-human species. Multiple structures within a chemical series are also important for establishing SAR.

C–C motif chemokine receptor 6 (CCR6) is expressed in dendritic and memory T cells and recruits pro-inflammatory IL-17-producing T cells to inflammation sites on skin or mucosa by activating heterotrimeric G_i or G_o protein. As such, it is a target for the treatment of inflammatory and autoimmune diseases, such as psoriasis and irritable bowel syndrome. In 2020, the first cryo-EM structure was reported of CCR6 bound to its activator, the C–C chemokine CCL20, with an engineered mini-G_O protein complex stabilized by scFv16 [32]. This structure, the first ever of an agonist peptide-bound chemokine receptor, revealed a novel activation mechanism. The CCL20 ligand binds an unusually shallow pocket (Figure 1B), making minimal contacts with the transmembrane helices of CCR6. This binding event allosterically activates a non-canonical toggle switch formed by residues Q267, Y125, and N271, over 15 Å from the binding site. Breaking hydrogen-bonding interactions between these residues induce the opening of helices 6 and 7, required for G protein binding. The mechanism revealed by this structure helped to explain prior mutagenesis studies, showing that extensive ligand–receptor contact is not required for activation, and highlighted the broad array of ligand-binding modes accommodated by GPCRs. Compounds mimicking the active CCL20 peptide could be designed to take advantage of the same interactions in this shallow pocket to act as agonists, or conversely, could be modified to inhibit CCR6 activity.

Ion channels

Given their high symmetry, ion channels enabled some of the earliest high-resolution cryo-EM structures [33,34]. They are also therapeutically important, being involved in a broad array of processes. Academic groups and companies, including Pfizer, Genentech, and Novartis, have reported novel cryo-EM structures of therapeutically relevant channels in recent years [35–39]. For instance, of therapeutic interest as sensory modulators, the transient receptor potential vanilloid (TRPV) channels form a family of six ligand-gated calcium channels in humans. Known for their role in heat sensation (thermoTRPV sub-family; TRPV2, 3, and 4), they are also modulated by natural ligands including capsaicin and cannabinoids. The first structures of TRPV-family channels, TRPV1 and TRPV2, were determined by cryo-EM in 2013 and 2016 [34,40], respectively, and more recent work has elucidated the structures of several other family members [41–44].

TRPV5 offers a useful example of how structural information, even at moderate resolution, can provide useful mechanistic information. Found in the apical membrane of kidney distal tubule epithelial cells (alongside the more ubiquitous TRPV6), TRPV5 is critical for calcium reabsorption and is linked to kidney stones. TRPV5/6 are constitutively active, but are modulated by intracellular ligands, including calmodulin and PIP_2. Two common topical antifungals, econazole, and miconazole, were found to inhibit the activities of both TRPV5 and TRPV6 [45,46]. The restricted tissue distribution of TRPV5, however, makes it a more attractive therapeutic target. In 2018, the structure of TRPV5 bound to econazole was determined by cryo-EM at 4.8 Å, with regions near the core reaching 3.5 Å [44]. Econazole binds a hydrophobic pocket normally bound by phosphoinositides and vanilloids in the related TRPV1 channel (Figure 1C). Despite the structure's relatively low resolution, molecular dynamics simulations and comparison to the capsazepine-bound structure of TRPV1 [47] allowed the ligand's binding site and inhibitory mechanism to be inferred, suggesting inhibitor binding was associated with movements in the S1–S4 helical bundle and the S4–S5 linker, rearranging a loop with key residues (M578, F574, and H582) that rotate into the pore to block ion flow. When mutated, residues flanking the econazole binding site reduced its inhibitory activity in a two-electrode voltage clamp assay in *Xenopus* oocytes, increasing confidence in its interactions and mechanism of action. Knowledge of key interactions in the ligand-binding pocket can also be used to design more potent and selective compounds.

While many membrane proteins are solubilized in detergents for structural solution, the compatibility of cryo-EM with other solubilization tools, such as nanodiscs [48], amphipols, peptidiscs, and styrene-maleic acid copolymers (SMALPs), can reduce structural perturbations and preserve critical protein–lipid interactions. Understanding such interactions can help to elucidate mechanistic details of protein function and identify potentially druggable pockets. TRPV2 plays important roles in neuronal development, cardiac function, immunity and cancer. Cannabidiol (CBD), a channel agonist, inhibits cell proliferation in glioblastoma multiforme, making TRPV2 an attractive anti-cancer target [49]. Several structures of TRPV channels in their apo forms, determined by cryo-EM and crystallography, suggested multiple potential ligand-binding sites, including

Biochemical Society Transactions (2021) **49** 2627–2638
https://doi.org/10.1042/BST20210444

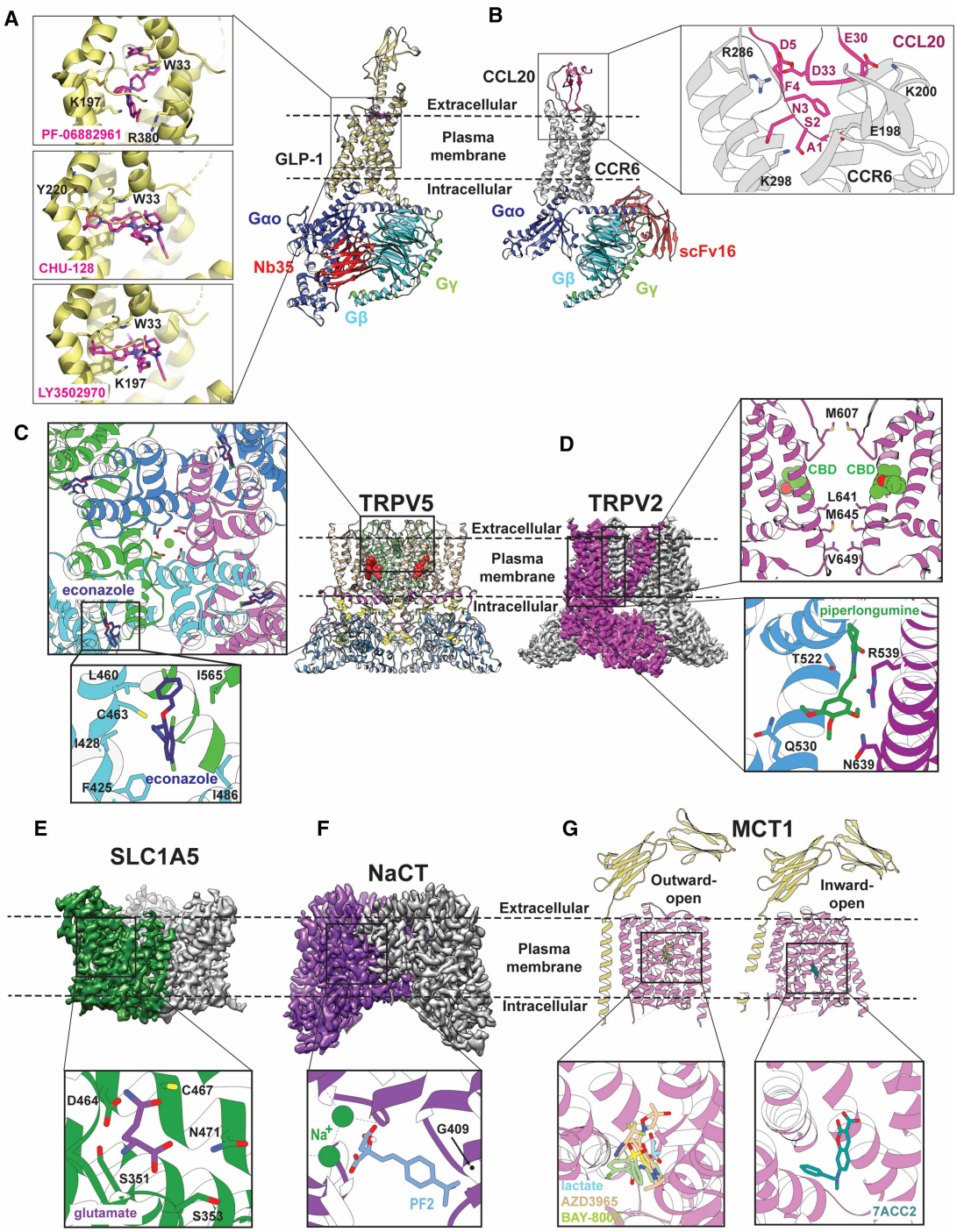

Figure 1. Liganded GPCR, ion channel, and solute carrier protein structures solved by cryo-EM. Part 1 of 2

(**A**,**B**) GPCRs: (**A**) Ligand-bound GLP-1 structures. *Right panel*, Structure of GLP-1 signaling complex (PDB 6X19), as solved by Sexton and colleagues [31], bound to CHU-128. *Upper left inset*, Structure of the ligand-binding pocket of GLP-1R bound to PF-06882961 [31]. *Middle left inset*, Structure of the ligand-binding pocket of GLP-1R bound to CHU-128. *Lower left inset*, Structures of the ligand-binding pocket of GLP-1R bound to LY3502970 [95]. (**B**) CCL20 peptide-bound CCR6 structure. *Left panel*, Cartoon representation of CCR6-G protein complex bound to CCL20 (PDB 6WWZ). *Right inset*, CCR6-CCL20 interaction interface with key interacting residues indicated. (**C**,**D**) Ion channels: (**C**) Econazole-bound structure of TRPV5 channel. *Right panel*, Structure of tetrameric TRPV5, colored by domain, bound to econazole (PDB 6B5V). *Upper left inset*, TRPV5 calcium-binding selectivity filter, colored by subunit, formed by D542 (shown in stick representation) from each subunit.

Figure 1. Liganded GPCR, ion channel, and solute carrier protein structures solved by cryo-EM. Part 2 of 2

Bound calcium ion is indicated in green and econazole shown in blue stick representation. *Lower left inset*, Econazole binding site. Side chains within 4.0 Å of the ligand during MD simulations are labeled and shown as sticks. (**D**) Liganded structures of TRPV2 channel. *Left panel*, Cryo-EM map for TRPV2 tetramer (EMD-20686) state 1 bound to cannabidiol (CBD), with a single subunit colored in violet and other subunits in gray. *Upper right inset*, Close-up of CBD binding site, with TRPV2 model cartoon (PDB 6U8A) shown in violet and CBD in space-filling representation shown in green. Residues forming the ion pore are indicated. *Lower right inset*, Piperlongumine binding site of TRPV2 (PDB 6WKN [53]), with TRPV2 cartoon colored by subunit and piperlongumine in stick representation. Key interacting residues are shown as sticks. (**E–G**) Solute carriers: (**E**) Substrate-bound structure of SLC1A5. *Upper panel*, Cryo-EM map for SLC1A5 trimer bound to glutamate (EMD-9188), with one subunit highlighted in green. *Lower inset*, Glutamate binding site of SLC1A5 in the outward-facing conformation (PDB 6MPB), with protein shown as cartoon in green, with glutamate in violet and interacting residues shown as sticks. (**F**) Structure of ligand-bound NaCT. *Upper panel*, Cryo-EM map of dimeric NaCT-PF-2 complex (EMD-22456), with one subunit colored in purple. *Lower inset*, Close-up of PF2 binding site, with NaCT shown in cartoon representation (purple, PDB 7JSJ), and compound and sodium ions colored as indicated. (**G**) Structures of MCT1 stabilized by ligands in outward- and inward-open conformations. *Upper panels*, Cartoon representations of MCT1 (pink)/basigin-2 (beige) complex in outward-open (*left*, PDB 6LYY) and inward-open (*right*, PDB 7CKO) conformations. *Lower panels*, Close-ups of compound-binding sites in outward-open (*left*, compounds superimposed and colored as indicated) and inward-open (*right*) states.

some occupied naturally by lipids [41,44,47,50,51]. In 2019, cryo-EM structures were reported of nanodisc-bound rat TRPV2 in two unliganded conformations and two bound to CBD [52]. These structures revealed CBD in a novel binding site (Figure 1D) between helices S5 and S6 of adjacent subunits in non-conducting conformations (pre-open or desensitized states). This novel binding site offers avenues for SBDD based on this scaffold. Interestingly, both the apo and liganded maps contained ordered density attributed to bound lipids, as seen in other TRPV channel structures. Electrophysiological studies revealed the channel to be active in the presence of CBD when reconstituted in liposomes, but to open occasionally for extended periods even in the apo form, suggesting membrane lipids may modulate its activity. A follow-up structure of TRPV2 was reported this year in the presence of piperlongumine, a naturally occurring alkaloid with selective anti-cancer properties [53]. Notably, the activity of piperlongumine was predicted computationally using SPIDER, a tool used to identify associations between small molecules and their protein targets, and it was subsequently validated *in vivo* as a TRPV2 antagonist. The cryo-EM structure of TRPV2 bound to piperlongumine identified a transient binding site, normally occupied by lipid, in the interface between two subunits (Figure 1D). Binding results in potent allosteric antagonism of TRPV2 activity and offers an alternative avenue for TRPV2 inhibition, while further highlighting the importance of lipid binding sites on its transmembrane surface for modulating its activity.

Solute carrier proteins

SLCs have emerged in recent years as a promising class of drug targets. Comprising facilitated transporters, antiporters, and symporters, SLCs are mechanistically diverse, and cryo-EM has been critical in teasing out their mechanisms of action, with significant implications for the druggability of this family. Three recent structures, solved by cryo-EM, highlight the diversity of this class of transporters while opening design opportunities for more potent and selective small-molecule inhibitors.

SLC1A5, a trimeric sodium-dependent amino acid antiporter, is the only SLC1 family member that transports glutamine, and serves as the primary glutamine transporter in cancer cells. Its inhibition reduces endometrial cancer cell growth and induces rapid cell death in breast cancer cells, making it a promising anti-cancer target. To elucidate its transport mechanism, cryo-EM structures of SLC1A5 were determined in its apo and L-glutamine-bound forms (Figure 1E) [54], which adopt an outward-facing conformation. This made SLC1A5 the first eukaryotic sodium-dependent neutral amino acid transporter to be solved in both inward and outward-facing states by cryo-EM [54,55]. Taken together, these structures revealed conformational changes underlying a finely tuned 'elevator' transport mechanism mediated by independently functioning protomers, in which each protomer's substrate-binding transport domain moves relative to a scaffold domain to carry substrate across the membrane. This mechanism is made possible by conformational changes in the HP2 loop, which serves as an extracellular gate controlling substrate access. This ensemble of structures clarified

Biochemical Society Transactions (2021) **49** 2627–2638
https://doi.org/10.1042/BST20210444

the molecular determinants of substrate recognition and engagement, insights that would be critical to inhibitor design.

NaCT/SLC13A5, a sodium-dependent citrate transporter found in the liver with an important role in citrate homeostasis, is one of three SLC13 family dicarboxylate transporters. Citrate's central role in carbon metabolism, particularly as an acyl-CoA precursor for fatty acid synthesis, makes NaCT an important target for treating obesity, and NaCT is often elevated in patients with non-alcoholic fatty liver disease. This year, cryo-EM structures of NaCT bound to citrate, as well as a potent and selective inhibitor, PF-06649298 (PF2), were reported, revealing its sodium-dependent elevator mechanism [56] (Figure 1F). Citrate binds in a basic pocket flanked by two SNT motifs that co-ordinate its carboxylate moieties. Mutations in these SNT motifs abolish transport activity. Moreover, density for two of the four sodium ions required for transport was discernable in the map. PF2, a competitive inhibitor, contains two carboxylate moieties that occupy the citrate binding pocket of NaCT in the inhibitor-bound structure, while key interactions with the NaCT scaffold domain block the sliding of the transport domain to the outward conformation, explaining the basis of its inhibition. Importantly, key side chains neighboring the inhibitor binding site, G409 and A57, are replaced by bulkier residues in other SLC13 family members that would clash with the inhibitor, which helped to rationalize its selectivity for NaCT. Indeed, mutation of G409 to asparagine, as found in orthologs, significantly reduced PF2 potency. These insights could inform the design of inhibitors with improved selectivity and potency.

MCT1 (also called SLC16A1), one of four proton-coupled transporters that catalyze the transport of monocarboxylates (such as lactate, pyruvate, ketone bodies), is part of a shuttling system that maintains lactate homeostasis between glycolytic and oxidative cells. Given its enhanced expression in some tumors, with a possible role in 'metabolic symbiosis' (extracellular lactic acid can confer immune tolerance), MCT1 is an important target for the treatment of cancer. This year, Wang et al. [57] reported 5 cryo-EM structures of MCT1 with its partner basigin-2, bound to lactate and several inhibitors. While the inhibitors bound the orthosteric site, these structures revealed multiple modes of inhibition, with MCT1 adopting the outward-open conformation in the presence of lactate and inhibitors BAY-8002 and AZD3965 (Figure 1G, left panel and inset), but an inward-open conformation when bound to inhibitor 7ACC2 (Figure 1F, right panel and inset). These structures revealed a transport mechanism by which relative rigid-body rotations of two domains expose substrate-binding sites alternately to opposite sides of the membrane. More importantly, this study identified the molecular determinants for subtype-specific sensitivities to AZD3965, which is currently in Phase I clinical trials for the treatment of cancer, by MCT1 and MCT4, critical for optimizing inhibitor selectivity [58].

Vaccines

Cryo-EM is a powerful tool in vaccine development to enable better antigen design, map epitopes through analysis of antibody–epitope complexes, and illuminate the molecular basis of vaccine efficacy. While vaccine efficacy relies on a host of factors, a key element is the design of an immunogen that will provoke a strong and lasting immune reaction. Human cytomegalovirus (HCMV), which commonly infects the human central nervous system, can cause severe disorders in immunocompromised carriers. Vaccines against HCMV have typically targeted glycoprotein B, which mediates membrane fusion with the host cell during viral entry, but their protection is often short-lived. For several viruses, its pre-fusion conformation has proven more effective at eliciting neutralizing antibodies, but the pre-fusion conformation of HCMV gB is unstable. To stabilize gB in its pre-fusion conformation, Liu et al. purified the protein from virions with an HCMV-specific fusion inhibitor, WAY-174865, [59,60], and crosslinked the protein to rigidify its conformation for cryo-EM. While successful in stabilizing the pre-fusion conformation (Figure 2A), this strategy did not prevent all particles from transitioning to post-fusion conformation. As a result, both the conformations were present in the sample, allowing structural solutions for both from a single dataset, at 3.6 Å and 3.5 Å, respectively [61]. Critically, the pre-fusion structure was congruent with models derived from cryo-electron tomography studies of intact viruses (Figure 2A, left panel) [62–64]. WAY-174865 ligand density was discernable in the pre-fusion conformation, revealing its mode of inhibition and the underlying mechanisms of inhibition escape mutations (Figure 2A, inset). On the basis of this evidence, it was concluded to represent a genuine pre-fusion conformation of HCMV gB. Neutralizing antibody epitopes were mapped onto the protein surface, reinforcing the hypothesis that interference with gH/gL binding is a potential mechanism of neutralization. Given that the reversibility of WAY-174865 binding makes it unsuitable as a vaccine stabilizer, these structures also offered the possibility of designing an inhibitor-free pre-fusion-stabilized vaccine antigen.

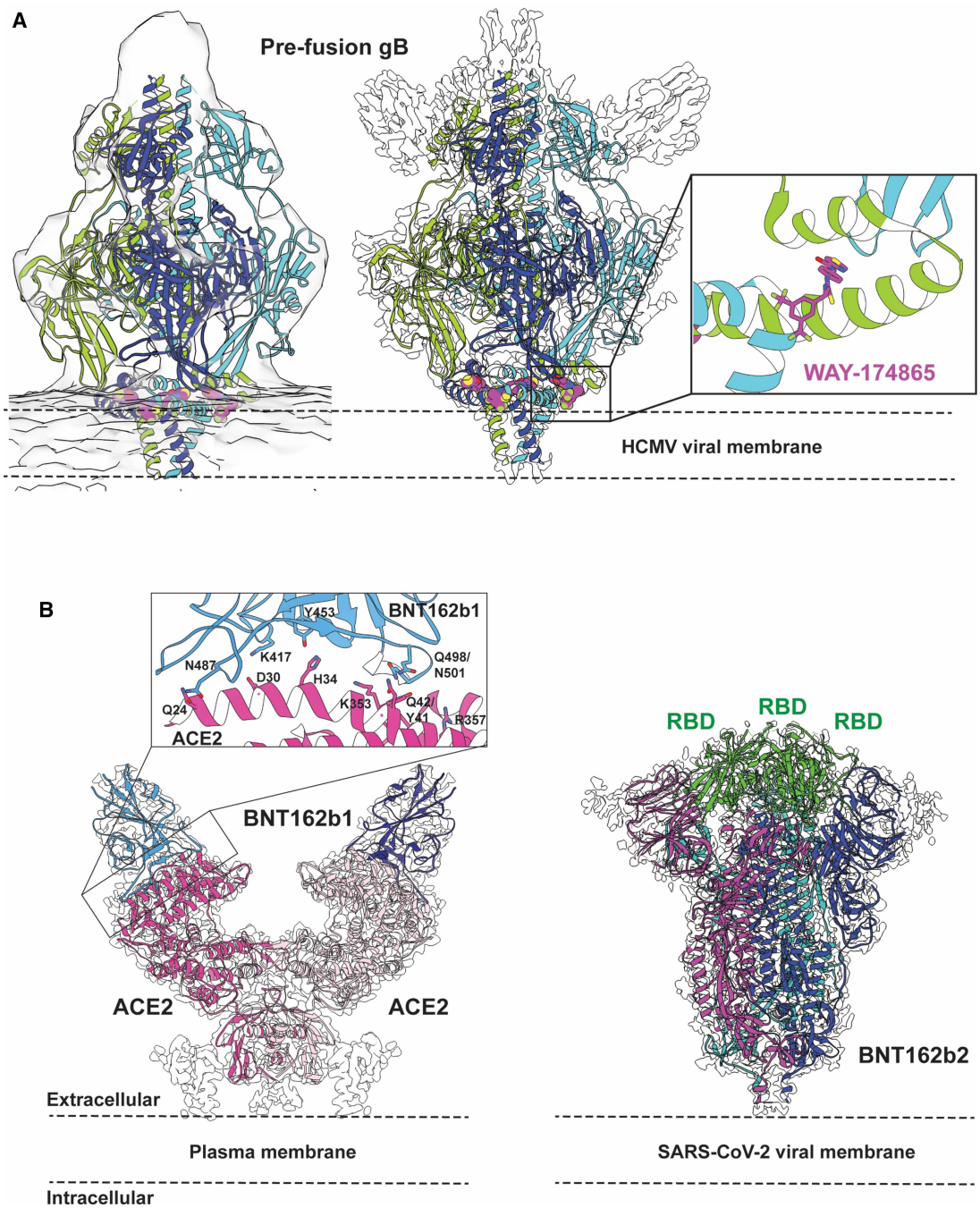

Figure 2. Cryo-EM structures for vaccine development.

(**A**) Cryo-EM structure of trimeric pre-fusion-stabilized HCMV gB, shown in cartoon representation bound to WAY-174865 (PDB 7KDP), superimposed with tomographic reconstruction [62] (EMD-9328; *left panel*) and its single-particle cryo-EM map [61] (EMD-22828; *middle panel*). Three unmodeled regions of density in the map correspond to a Fab fragment from a neutralizing antibody (SM5-1) against gB. *Right inset*, WAY-174865 binding pocket in gB trimer. (**B**) Cryo-EM structures of SARS-CoV-2 vaccine antigens BNT162b1 and BNT162b2. *Left panel*, Cryo-EM structure of dimeric ACE2 (pink) bound to two copies of BNT162b1-encoded SARS-CoV-2 spike protein RBD (blue, PDB 7L7F), superimposed with its cryo-EM map (EMD-23211). Inset shows ACE2-RBD binding interface, with key residues highlighted. *Right panel*, Cryo-EM structure of trimeric pre-fusion-stabilized SARS-CoV-2 spike protein (PDB 7L7K) encoded by BNT162b2, superimposed with its cryo-EM density (EMD-23215). Subunits are individually colored, with RBD domains separately colored in green.

Biochemical Society Transactions (2021) **49** 2627–2638
https://doi.org/10.1042/BST20210444

Cryo-EM has also long been invaluable for identifying protein epitopes bound by antibodies, which is useful for designing vaccines and understanding the factors underlying their efficacy. In early 2020, as a novel SARS coronavirus, which causes COVID19, emerged as a global public health threat, Pfizer, collaborating with German firm BioNTech, rapidly mobilized to develop a novel mRNA-based vaccine that would deliver viral spike protein-coding sequences to patient cells. Two major candidate antigens were evaluated. BNT162b1 encoded an artificially trimerized version of the spike protein receptor-binding domain (RBD), in contrast with a pre-fusion-stabilized version of the full-length spike protein (BNT162b2). Given the novelty of mRNA-based vaccines, structural characterization was critical to ensure the correct epitopes are presented to patients' immune systems. To enable antigen characterization by cryo-EM, the small and flexible RBD trimer encoded by BNT162b1 was combined with the human receptor for the spike protein, ACE2, which improved its size and rigidity. The structure of this complex revealed that the RBD trimer adopts its active fold and binds to the receptor via its native interface (Figure 2B left panel), making it effective in stimulating neutralizing antibody production. The structure of BNT162b2, which ultimately formed the basis of the vaccine now in use, revealed not only its native conformation (Figure 2B right panel), but also highlighted the conformational dynamics of the RBDs, whose conformations are critical to vaccine efficacy [65]. Pfizer/BioNTech's COVID19 vaccine, which was granted emergency use authorization by the US FDA in December 2020 and full approval in August 2021, is currently in use around the world to help control the spread of COVID19.

The future of cryo-EM in drug discovery

Cryo-EM technology continues to evolve rapidly and its user base is expanding rapidly. The costs of equipment and maintenance and the computational requirements of data processing, which have been hurdles to more widespread adoption, are being addressed by the development of smaller, less-costly microscopes, the establishment of government-funded cryo-EM data collection centers, and the growing use and availability of cloud computing resources [66,67]. Recent publications suggest that the newer generation of smaller, less costly microscopes are becoming capable of routinely producing high-resolution structures, encouraging new entrants to the field [68–70].

In an industrial setting, it must be possible to iteratively determine high-resolution liganded structures to enable SBDD. For cryo-EM to play this role, each step, from sample preparation to data processing, must be optimized for rapid structural solutions. Preparation of high-quality samples will likely remain the rate-determining step for many cryo-EM structures, but new sample deposition technologies, with prominent examples being the Spotiton method (supported by the Chameleon system and self-blotting grids) [71–73] and the Vitrojet system [74] offer greater control of sample deposition on grids, while allowing quality assessment on the fly to reduce grid screening time. Furthermore, data acquisition software now offers automated hole and ice thickness assessment, selecting the best ice for data collection [75,76]. The newest generation of direct electron detectors, which boast high frame rates and increasingly stable and effective energy filters, improve micrograph signal-to-noise ratios to allow high-resolution reconstructions from fewer particles [77], reducing the data collection time per structure. The recently reported structures of β3 $GABA_A$ receptor at 1.7 Å and mouse apoferritin at 1.22 Å demonstrate the power of these technologies to enable true atomic-level structural details [78].

Increasingly sophisticated software has also accelerated the transition from dataset to structure, offering better tools for aberration correction [79,80], particle extraction [81–84], classification, and selection, and *de novo* 3D reconstruction [85], with increasing impacts from machine learning and artificial intelligence [81,82,84,86,87]. The use of maximum likelihood methods combined with GPU-enabled computation, as implemented in RELION, revolutionized the speed and accuracy of cryo-EM reconstructions from raw data [88,89]. The advent of on-the-fly data processing, implemented in tools such as CryoSPARC Live [85], now enables the assessment of dataset quality in 3D concurrently with data collection. As the selection of grids, ice, and particles becomes better optimized, the computational burden of filtering good from bad particles is reduced, and we anticipate that further streamlining will continue to reduce computational needs and speed data processing. Recent iterations of data processing software have included improved tools for processing particles with inter-domain flexibility or conformational changes, even in the absence of discrete structural states, allowing higher-resolution modeling of proteins in multiple conformations and analysis of their conformational dynamics [90–92], with even time-resolved structures beginning to emerge [93,94].

In the longer term, improvements in both hardware and software to support cryo-electron tomography are expected to better enable the imaging of proteins in their native cellular context at high resolution. Eventually,

particle picking algorithms may allow the effective extraction of single particles *in situ* from images of cells thinned by focused ion beam (FIB) milling for single-particle analysis [83]. This approach offers the advantage of true native conditions without protein purification, which could eliminate a major bottleneck to structure determination. While this technology is still under development, rapid improvements may soon make it an important part of the structural biologist's toolbox.

Despite the rapid growth of cryo-EM and the development of powerful new tools, the preparation of more inherently challenging samples and intensive computational work makes certain tasks like the iterative solution of ligand-bound structures more difficult with cryo-EM. X-ray crystallography still excels where repeated structure determinations need to be made. SBDD benefits from structures at the highest resolutions possible, with the ability to resolve atomic positions and confidently place ordered water molecules with high accuracy. In this sense, the use of cryo-EM for SBDD remains in its infancy except for the limited number of well-validated samples. Technological development to address these limitations in the coming years will be key to establishing cryo-EM firmly in drug discovery pipelines across the industry. The remarkable achievements of the past few years, however, suggest that the fruition of this reality may be closer than we think.

Perspective

- Cryo-EM has become an indispensable structural biology tool, accounting for a growing percentage of newly solved protein structures.
- Cryo-EM has enabled structural analysis of challenging drug targets to support SBDD, driving the development of novel therapeutics, including biologics.
- Technological innovations continue to increase the power of cryo-EM in drug discovery, positioning it to play a major role in pharmaceutical development going forward.

Competing Interests

J.A.L., J.M.D., and S.H. are employed by Pfizer and may hold Pfizer stock or stock options.

Author Contributions

J.A.L., J.M.D., and S.H. wrote and edited the article.

Abbreviations

CBD, cannabidiol; CCR6, C–C motif chemokine receptor 6; cryo-EM, cryo-electron microscopy; $GABA_B$, γ-aminobutyric acid type B; GLP-1R, glucagon-like peptide 1 receptor; GPCRs, G protein-coupled receptors; HCMV, human cytomegalovirus; RBD, receptor-binding domain; SAR, structure–activity relationship; SBDD, structure-based drug design; SLCs, solute carriers; TRPV, transient receptor potential vanilloid.

References

1 Robertson, M.J., Meyerowitz, J.G. and Skiniotis, G. (2021) Drug discovery in the era of cryo-electron microscopy. *Trends Biochem. Sci.* **S0968-0004 (21)00142-0** https://doi.org/10.1016/j.tibs.2021.06.008
2 Renaud, J.P., Chari, A., Ciferri, C., Liu, W.T., Remigy, H.W., Stark, H. et al. (2018) Cryo-EM in drug discovery: achievements, limitations and prospects. *Nat. Rev. Drug Discov.* **17**, 471–492 https://doi.org/10.1038/nrd.2018.77
3 Overington, J.P., Al-Lazikani, B. and Hopkins, A.L. (2006) How many drug targets are there? *Nat. Rev. Drug Discov.* **5**, 993–996 https://doi.org/10.1038/nrd2199
4 Yin, H. and Flynn, A.D. (2016) Drugging membrane protein interactions. *Annu. Rev. Biomed. Eng.* **18**, 51–76 https://doi.org/10.1146/annurev-bioeng-092115-025322
5 Salon, J.A., Lodowski, D.T. and Palczewski, K. (2011) The significance of G protein-coupled receptor crystallography for drug discovery. *Pharmacol. Rev.* **63**, 901–937 https://doi.org/10.1124/pr.110.003350
6 Santos, R., Ursu, O., Gaulton, A., Bento, A.P., Donadi, R.S., Bologa, C.G. et al. (2017) A comprehensive map of molecular drug targets. *Nat. Rev. Drug Discov.* **16**, 19–34 https://doi.org/10.1038/nrd.2016.230
7 Kooistra, A.J., Mordalski, S., Pandy-Szekeres, G., Esguerra, M., Mamyrbekov, A., Munk, C. et al. (2021) GPCRdb in 2021: integrating GPCR sequence, structure and function. *Nucleic Acids Res.* **49**, D335–D343 https://doi.org/10.1093/nar/gkaa1080
8 McManus, O.B. (2014) HTS assays for developing the molecular pharmacology of ion channels. *Curr. Opin. Pharmacol.* **15**, 91–96 https://doi.org/10.1016/j.coph.2014.01.004

9 Wang, W.W., Gallo, L., Jadhav, A., Hawkins, R. and Parker, C.G. (2020) The druggability of solute carriers. *J. Med. Chem.* **63**, 3834–3867 https://doi.org/10.1021/acs.jmedchem.9b01237
10 Bai, X., Moraes, T.F. and Reithmeier, R.A.F. (2017) Structural biology of solute carrier (SLC) membrane transport proteins. *Mol. Membr. Biol.* **34**, 1–32 https://doi.org/10.1080/09687688.2018.1448123
11 Estudante MS, G., Morais, J.G. and Benet, L.Z. (2016) Insights into solute carriers: physiological functions and implications in disease and pharmacokinetics. *Med. Chem. Commun.* **7**, 1462–1478 https://doi.org/10.1039/C6MD00188B
12 Schaller, L. and Lauschke, V.M. (2019) The genetic landscape of the human solute carrier (SLC) transporter superfamily. *Hum. Genet.* **138**, 1359–1377 https://doi.org/10.1007/s00439-019-02081-x
13 Lake, J.A. (1976) Ribosome structure determined by electron microscopy of *Escherichia coli* small subunits, large subunits and monomeric ribosomes. *J. Mol. Biol.* **105**, 131–139 https://doi.org/10.1016/0022-2836(76)90200-X
14 Patwardhan, A. (2017) Trends in the electron microscopy data bank (EMDB). *Acta Crystallogr. D Struct. Biol.* **73**(Pt 6), 503–508 https://doi.org/10.1107/S2059798317004181
15 Bottcher, B., Wynne, S.A. and Crowther, R.A. (1997) Determination of the fold of the core protein of hepatitis B virus by electron cryomicroscopy. *Nature* **386**, 88–91 https://doi.org/10.1038/386088a0
16 Conway, J.F., Cheng, N., Zlotnick, A., Wingfield, P.T., Stahl, S.J. and Steven, A.C. (1997) Visualization of a 4-helix bundle in the hepatitis B virus capsid by cryo-electron microscopy. *Nature* **386**, 91–94 https://doi.org/10.1038/386091a0
17 Maeda, S., Koehl, A., Matile, H., Hu, H., Hilger, D., Schertler, G.F.X. et al. (2018) Development of an antibody fragment that stabilizes GPCR/G-protein complexes. *Nat. Commun.* **9**, 3712 https://doi.org/10.1038/s41467-018-06002-w
18 Rasmussen, S.G., DeVree, B.T., Zou, Y., Kruse, A.C., Chung, K.Y., Kobilka, T.S. et al. (2011) Crystal structure of the beta2 adrenergic receptor-Gs protein complex. *Nature* **477**, 549–555 https://doi.org/10.1038/nature10361
19 Carpenter, B. and Tate, C.G. (2016) Engineering a minimal G protein to facilitate crystallisation of G protein-coupled receptors in their active conformation. *Protein Eng. Des. Sel.* **29**, 583–594 https://doi.org/10.1016/j.aca.2019.12.036
20 Liang, Y.L., Zhao, P., Draper-Joyce, C., Baltos, J.A., Glukhova, A., Truong, T.T. et al. (2018) Dominant negative g proteins enhance formation and purification of agonist-GPCR-G protein complexes for structure determination. *ACS Pharmacol. Transl. Sci.* **1**, 12–20 https://doi.org/10.1021/acsptsci.8b00017
21 Mukherjee, S., Erramilli, S.K., Ammirati, M., Alvarez, F.J.D., Fennell, K.F., Purdy, M.D. et al. (2020) Synthetic antibodies against BRIL as universal fiducial marks for single-particle cryoEM structure determination of membrane proteins. *Nat. Commun.* **11**, 1598 https://doi.org/10.1038/s41467-020-15363-0
22 Papasergi-Scott, M.M., Robertson, M.J., Seven, A.B., Panova, O., Mathiesen, J.M. and Skiniotis, G. (2020) Structures of metabotropic GABAB receptor. *Nature* **584**, 310–314 https://doi.org/10.1038/s41586-020-2469-4
23 Mao, C., Shen, C., Li, C., Shen, D.D., Xu, C., Zhang, S. et al. (2020) Cryo-EM structures of inactive and active GABAB receptor. *Cell Res.* **30**, 564–573 https://doi.org/10.1038/s41422-020-0350-5
24 Kim, Y., Jeong, E., Jeong, J.H., Kim, Y. and Cho, Y. (2020) Structural basis for activation of the heterodimeric GABAB receptor. *J. Mol. Biol.* **432**, 5966–5984 https://doi.org/10.1016/j.jmb.2020.09.023
25 Seven, A.B., Barros-Alvarez, X., de Lapeyriere, M., Papasergi-Scott, M.M., Robertson, M.J., Zhang, C. et al. (2021) G-protein activation by a metabotropic glutamate receptor. *Nature* **595**, 450–454 https://doi.org/10.1038/s41586-021-03680-3
26 Wen, T., Wang, Z., Chen, X., Ren, Y., Lu, X., Xing, Y. et al. (2021) Structural basis for activation and allosteric modulation of full-length calcium-sensing receptor. *Sci. Adv.* **7**, eabg1483 https://doi.org/10.1126/sciadv.abg1483
27 Gao, Y., Robertson, M.J., Rahman, S.N., Seven, A.B., Zhang, C., Meyerowitz, J.G. et al. (2021) Asymmetric activation of the calcium-sensing receptor homodimer. *Nature* **595**, 455–459 https://doi.org/10.1038/s41586-021-03691-0
28 Zhang, Y., Sun, B., Feng, D., Hu, H., Chu, M., Qu, Q. et al. (2017) Cryo-EM structure of the activated GLP-1 receptor in complex with a G protein. *Nature* **546**, 248–253 https://doi.org/10.1038/nature22394
29 Liang, Y.L., Khoshouei, M., Glukhova, A., Furness, S.G.B., Zhao, P., Clydesdale, L. et al. (2018) Phase-plate cryo-EM structure of a biased agonist-bound human GLP-1 receptor-Gs complex. *Nature* **555**, 121–125 https://doi.org/10.1038/nature25773
30 Griffith, D.A., Edmonds, D.J., Fortin, J.-P., Kalgutkar, A.S., Brent Kuzmiski, J., Loria, P.M. et al. (2020) A small-molecule oral agonist of the human glucagon-like peptide-1 receptor. *bioRxiv*
31 Zhang, X., Belousoff, M.J., Zhao, P., Kooistra, A.J., Truong, T.T., Ang, S.Y. et al. (2020) Differential GLP-1R binding and activation by peptide and non-peptide agonists. *Mol. Cell* **80**, 485–500.e7 https://doi.org/10.1016/j.molcel.2020.09.020
32 Wasilko, D.J., Johnson, Z.L., Ammirati, M., Che, Y., Griffor, M.C., Han, S. et al. (2020) Structural basis for chemokine receptor CCR6 activation by the endogenous protein ligand CCL20. *Nat. Commun.* **11**, 3031 https://doi.org/10.1038/s41467-020-16820-6
33 Cao, E., Liao, M., Cheng, Y. and Julius, D. (2013) TRPV1 structures in distinct conformations reveal activation mechanisms. *Nature* **504**, 113–118 https://doi.org/10.1038/nature12823
34 Liao, M., Cao, E., Julius, D. and Cheng, Y. (2013) Structure of the TRPV1 ion channel determined by electron cryo-microscopy. *Nature* **504**, 107–112 https://doi.org/10.1038/nature12822
35 Liu, C., Reese, R., Vu, S., Rouge, L., Shields, S.D., Kakiuchi-Kiyota, S. et al. (2021) A Non-covalent ligand reveals biased agonism of the TRPA1 ion channel. *Neuron* **109**, 273–284.e4 https://doi.org/10.1016/j.neuron.2020.10.014
36 Kschonsak, M., Chua, H.C., Noland, C.L., Weidling, C., Clairfeuille, T., Bahlke, O.O. et al. (2020) Structure of the human sodium leak channel NALCN. *Nature* **587**, 313–318 https://doi.org/10.1038/s41586-020-2570-8
37 Clairfeuille, T., Cloake, A., Infield, D.T., Llongueras, J.P., Arthur, C.P., Li, Z.R. et al. (2019) Structural basis of alpha-scorpion toxin action on Nav channels. *Science* **363**, eaav8573 https://doi.org/10.1126/science.aav8573
38 Xu, H., Li, T., Rohou, A., Arthur, C.P., Tzakoniati, F., Wong, E. et al. (2019) Structural basis of Nav1.7 inhibition by a gating-modifier spider toxin. *Cell* **176**, 1238–1239 https://doi.org/10.1016/j.cell.2019.01.047
39 Dickson, C.J., Velez-Vega, C. and Duca, J.S. (2020) Revealing molecular determinants of herg blocker and activator binding. *J. Chem. Inf. Model.* **60**, 192–203 https://doi.org/10.1021/acs.jcim.9b00773

40 Huynh, K.W., Cohen, M.R., Jiang, J., Samanta, A., Lodowski, D.T., Zhou, Z.H. et al. (2016) Structure of the full-length TRPV2 channel by cryo-EM. *Nat. Commun.* **7**, 11130 https://doi.org/10.1038/ncomms11130
41 Singh, A.K., McGoldrick, L.L. and Sobolevsky, A.I. (2018) Structure and gating mechanism of the transient receptor potential channel TRPV3. *Nat. Struct. Mol. Biol.* **25**, 805–813 https://doi.org/10.1038/s41594-018-0108-7
42 Deng, Z., Paknejad, N., Maksaev, G., Sala-Rabanal, M., Nichols, C.G., Hite, R.K. et al. (2018) Cryo-EM and X-ray structures of TRPV4 reveal insight into ion permeation and gating mechanisms. *Nat. Struct. Mol. Biol.* **25**, 252–260 https://doi.org/10.1038/s41594-018-0037-5
43 Saotome, K., Singh, A.K., Yelshanskaya, M.V. and Sobolevsky, A.I. (2016) Crystal structure of the epithelial calcium channel TRPV6. *Nature* **534**, 506–511 https://doi.org/10.1038/nature17975
44 Hughes, T.E.T., Lodowski, D.T., Huynh, K.W., Yazici, A., Del Rosario, J., Kapoor, A. et al. (2018) Structural basis of TRPV5 channel inhibition by econazole revealed by cryo-EM. *Nat. Struct. Mol. Biol.* **25**, 53–60 https://doi.org/10.1038/s41594-017-0009-1
45 Na, T. and Peng, J.B. (2014) TRPV5: a Ca(2+) channel for the fine-tuning of Ca(2+) reabsorption. *Handb. Exp. Pharmacol.* **222**, 321–357 https://doi.org/10.1007/978-3-642-54215-2_13
46 Nilius, B., Prenen, J., Vennekens, R., Hoenderop, J.G., Bindels, R.J. and Droogmans, G. (2001) Pharmacological modulation of monovalent cation currents through the epithelial Ca^{2+} channel ECaC1. *Br. J. Pharmacol.* **134**, 453–462 https://doi.org/10.1038/sj.bjp.0704272
47 Gao, Y., Cao, E., Julius, D. and Cheng, Y. (2016) TRPV1 structures in nanodiscs reveal mechanisms of ligand and lipid action. *Nature* **534**, 347–351 https://doi.org/10.1038/nature17964
48 Denisov, I.G. and Sligar, S.G. (2016) Nanodiscs for structural and functional studies of membrane proteins. *Nat. Struct. Mol. Biol.* **23**, 481–486 https://doi.org/10.1038/nsmb.3195
49 Nabissi, M., Morelli, M.B., Santoni, M. and Santoni, G. (2013) Triggering of the TRPV2 channel by cannabidiol sensitizes glioblastoma cells to cytotoxic chemotherapeutic agents. *Carcinogenesis* **34**, 48–57 https://doi.org/10.1093/carcin/bgs328
50 McGoldrick, L.L., Singh, A.K., Saotome, K., Yelshanskaya, M.V., Twomey, E.C., Grassucci, R.A., et al. (2018) Opening of the human epithelial calcium channel TRPV6. *Nature* **553**, 233–237 https://doi.org/10.1038/nature25182
51 Zubcevic, L., Le, S., Yang, H. and Lee, S.Y. (2018) Conformational plasticity in the selectivity filter of the TRPV2 ion channel. *Nat. Struct. Mol. Biol.* **25**, 405–415 https://doi.org/10.1038/s41594-018-0059-z
52 Pumroy, R.A., Samanta, A., Liu, Y., Hughes, T.E., Zhao, S., Yudin, Y. et al. (2019) Molecular mechanism of TRPV2 channel modulation by cannabidiol. *eLife* **8**, e48792 https://doi.org/10.7554/eLife.48792
53 Conde, J., Pumroy, R.A., Baker, C., Rodrigues, T., Guerreiro, A., Sousa, B.B. et al. (2021) Allosteric antagonist modulation of TRPV2 by piperlongumine impairs glioblastoma progression. *ACS Cent. Sci.* **7**, 868–881 https://doi.org/10.1021/acscentsci.1c00070
54 Yu, X., Plotnikova, O., Bonin, P.D., Subashi, T.A., McLellan, T.J., Dumlao, D. et al. (2019) Cryo-EM structures of the human glutamine transporter SLC1A5 (ASCT2) in the outward-facing conformation. *eLife* **8**, e48120 https://doi.org/10.7554/elife.48120
55 Garaeva, A.A., Oostergetel, G.T., Gati, C., Guskov, A., Paulino, C. and Slotboom, D.J. (2018) Cryo-EM structure of the human neutral amino acid transporter ASCT2. *Nat. Struct. Mol. Biol.* **25**, 515–521 https://doi.org/10.1038/s41594-018-0076-y
56 Sauer, D.B., Song, J., Wang, B., Hilton, J.K., Karpowich, N.K., Mindell, J.A. et al. (2021) Structure and inhibition mechanism of the human citrate transporter NaCT. *Nature* **591**, 157–161 https://doi.org/10.1038/s41586-021-03230-x
57 Wang, N., Jiang, X., Zhang, S., Zhu, A., Yuan, Y., Xu, H. et al. (2021) Structural basis of human monocarboxylate transporter 1 inhibition by anti-cancer drug candidates. *Cell* **184**, 370–383.e13 https://doi.org/10.1016/j.cell.2020.11.043
58 Curtis, N.J., Mooney, L., Hopcroft, L., Michopoulos, F., Whalley, N., Zhong, H. et al. (2017) Pre-clinical pharmacology of AZD3965, a selective inhibitor of MCT1: DLBCL, NHL and Burkitt's lymphoma anti-tumor activity. *Oncotarget* **8**, 69219–69236 https://doi.org/10.18632/oncotarget.18215
59 Bloom, J.D., DiGrandi, M.J., Dushin, R.G., Curran, K.J., Ross, A.A., Norton, E.B. et al. (2003) Thiourea inhibitors of herpes viruses. Part 1: bis-(aryl) thiourea inhibitors of CMV. *Bioorg. Med. Chem. Lett.* **13**, 2929–2932 https://doi.org/10.1016/S0960-894X(03)00586-9
60 Bloom, J.D., Dushin, R.G., Curran, K.J., Donahue, F., Norton, E.B., Terefenko, E. et al. (2004) Thiourea inhibitors of herpes viruses. Part 2: N-Benzyl-N'-arylthiourea inhibitors of CMV. *Bioorg. Med. Chem. Lett.* **14**, 3401–3406 https://doi.org/10.1016/j.bmcl.2004.04.093
61 Liu, Y., Heim, K.P., Che, Y., Chi, X., Qiu, X., Han, S. et al. (2021) Prefusion structure of human cytomegalovirus glycoprotein B and structural basis for membrane fusion. *Sci. Adv.* **7**, eabf3178 https://doi.org/10.1126/sciadv.abf3178
62 Si, Z., Zhang, J., Shivakoti, S., Atanasov, I., Tao, C.L., Hui, W.H. et al. (2018) Different functional states of fusion protein gB revealed on human cytomegalovirus by cryo electron tomography with Volta phase plate. *PLoS Pathog.* **14**, e1007452 https://doi.org/10.1371/journal.ppat.1007452
63 Zeev-Ben-Mordehai, T., Vasishtan, D., Hernandez Duran, A., Vollmer, B., White, P., Prasad Pandurangan, A. et al. (2016) Two distinct trimeric conformations of natively membrane-anchored full-length herpes simplex virus 1 glycoprotein B. *Proc. Natl Acad. Sci. U.S.A.* **113**, 4176–4181 https://doi.org/10.1073/pnas.1523234113
64 Vollmer, B., Prazak, V., Vasishtan, D., Jefferys, E.E., Hernandez-Duran, A., Vallbracht, M. et al. (2020) The prefusion structure of herpes simplex virus glycoprotein B. *Sci. Adv.* **6**, eabc1726 https://doi.org/10.1126/sciadv.abc1726
65 Vogel, A.B., Kanevsky, I., Che, Y., Swanson, K.A., Muik, A., Vormehr, M. et al. (2021) BNT162b vaccines protect rhesus macaques from SARS-CoV-2. *Nature* **592**, 283–289 https://doi.org/10.1038/s41586-021-03275-y
66 Stuart, D.I., Subramaniam, S. and Abrescia, N.G. (2016) The democratization of cryo-EM. *Nat. Methods* **13**, 607–608 https://doi.org/10.1038/nmeth.3946
67 Naydenova, K., McMullan, G., Peet, M.J., Lee, Y., Edwards, P.C., Chen, S. et al. (2019) CryoEM at 100 keV: a demonstration and prospects. *IUCrJ* **6**(Pt 6), 1086–1098 https://doi.org/10.1107/S2052252519012612
68 Herzik MA, J., Wu, M. and Lander, G.C. (2019) High-resolution structure determination of sub-100 kDa complexes using conventional cryo-EM. *Nat. Commun.* **10**, 1032 https://doi.org/10.1038/s41467-019-08991-8
69 Wu, M., Lander, G.C. and Herzik, Jr, M.A. (2020) Sub-2 Angstrom resolution structure determination using single-particle cryo-EM at 200keV. *J. Struct. Biol. X* **4**, 100020 https://doi.org/10.1016/j.yjsbx.2020.100020
70 Merk, A., Fukumura, T., Zhu, X., Darling, J.E., Grisshammer, R., Ognjenovic, J. et al. (2020) 1.8 a resolution structure of beta-galactosidase with a 200 kV CRYO ARM electron microscope. *IUCrJ* **7**(Pt 4), 639–643 https://doi.org/10.1107/S2052252520006855
71 Razinkov, I., Dandey, V., Wei, H., Zhang, Z., Melnekoff, D., Rice, W.J. et al. (2016) A new method for vitrifying samples for cryoEM. *J. Struct. Biol.* **195**, 190–198 https://doi.org/10.1016/j.jsb.2016.06.001

72 Wei, H., Dandey, V.P., Zhang, Z., Raczkowski, A., Rice, W.J., Carragher, B. et al. (2018) Optimizing "self-wicking" nanowire grids. *J. Struct. Biol.* **202**, 170–174 https://doi.org/10.1016/j.jsb.2018.01.001
73 Dandey, V.P., Wei, H., Zhang, Z., Tan, Y.Z., Acharya, P., Eng, E.T. et al. (2018) Spotiton: new features and applications. *J. Struct. Biol.* **202**, 161–169 https://doi.org/10.1016/j.jsb.2018.01.002
74 Ravelli, R.B.G., Nijpels, F.J.T., Henderikx, R.J.M., Weissenberger, G., Thewessem, S., Gijsbers, A. et al. (2020) Cryo-EM structures from sub-nl volumes using pin-printing and jet vitrification. *Nat. Commun.* **11**, 2563 https://doi.org/10.1038/s41467-020-16392-5
75 Mastronarde, D.N. (2005) Automated electron microscope tomography using robust prediction of specimen movements. *J. Struct. Biol.* **152**, 36–51 https://doi.org/10.1016/j.jsb.2005.07.007
76 Tan, Y.Z., Cheng, A., Potter, C.S. and Carragher, B. (2016) Automated data collection in single particle electron microscopy. *Microscopy (Oxf.)* **65**, 43–56 https://doi.org/10.1093/jmicro/dfv369
77 Yip, K.M., Fischer, N., Paknia, E., Chari, A. and Stark, H. (2020) Atomic-resolution protein structure determination by cryo-EM. *Nature* **587**, 157–161 https://doi.org/10.1038/s41586-020-2833-4
78 Nakane, T., Kotecha, A., Sente, A., McMullan, G., Masiulis, S., Brown, P. et al. (2020) Single-particle cryo-EM at atomic resolution. *Nature* **587**, 152–156 https://doi.org/10.1038/s41586-020-2829-0
79 Zhang, K. (2016) Gctf: real-time CTF determination and correction. *J. Struct. Biol.* **193**, 1–12 https://doi.org/10.1016/j.jsb.2015.11.003
80 Rohou, A. and Grigorieff, N. (2015) CTFFIND4: fast and accurate defocus estimation from electron micrographs. *J. Struct. Biol.* **192**, 216–221 https://doi.org/10.1016/j.jsb.2015.08.008
81 Bepler, T., Morin, A., Rapp, M., Brasch, J., Shapiro, L., Noble, A.J. et al. (2019) Positive-unlabeled convolutional neural networks for particle picking in cryo-electron micrographs. *Nat. Methods* **16**, 1153–1160 https://doi.org/10.1038/s41592-019-0575-8
82 Tegunov, D. and Cramer, P. (2019) Real-time cryo-electron microscopy data preprocessing with Warp. *Nat. Methods* **16**, 1146–1152 https://doi.org/10.1038/s41592-019-0580-y
83 Rickgauer, J.P., Grigorieff, N. and Denk, W. (2017) Single-protein detection in crowded molecular environments in cryo-EM images. *eLife* **6**, e25648 https://doi.org/10.7554/eLife.25648
84 Bepler, T., Kelley, K., Noble, A.J. and Berger, B. (2020) Topaz-Denoise: general deep denoising models for cryoEM and cryoET. *Nat. Commun.* **11**, 5208 https://doi.org/10.1038/s41467-020-18952-1
85 Punjani, A., Rubinstein, J.L., Fleet, D.J. and Brubaker, M.A. (2017) cryoSPARC: algorithms for rapid unsupervised cryo-EM structure determination. *Nat. Methods* **14**, 290–296 https://doi.org/10.1038/nmeth.4169
86 Wagner, T., Merino, F., Stabrin, M., Moriya, T., Antoni, C., Apelbaum, A. et al. (2019) SPHIRE-crYOLO is a fast and accurate fully automated particle picker for cryo-EM. *Commun. Biol.* **2**, 218 https://doi.org/10.1038/s42003-019-0437-z
87 Wang, F., Gong, H., Liu, G., Li, M., Yan, C., Xia, T. et al. (2016) Deeppicker: a deep learning approach for fully automated particle picking in cryo-EM. *J. Struct. Biol.* **195**, 325–336 https://doi.org/10.1016/j.jsb.2016.07.006
88 Scheres, S.H. (2012) RELION: implementation of a Bayesian approach to cryo-EM structure determination. *J. Struct. Biol.* **180**, 519–530 https://doi.org/10.1016/j.jsb.2012.09.006
89 Kimanius, D., Forsberg, B.O., Scheres, S.H. and Lindahl, E. (2016) Accelerated cryo-EM structure determination with parallelisation using GPUs in RELION-2. *eLife* **5**, e18722 https://doi.org/10.7554/eLife.18722
90 Punjani, A., Zhang, H. and Fleet, D.J. (2020) Non-uniform refinement: adaptive regularization improves single-particle cryo-EM reconstruction. *Nat. Methods* **17**, 1214–1221 https://doi.org/10.1038/s41592-020-00990-8
91 Punjani, A. and Fleet, D.J. (2021) 3D variability analysis: resolving continuous flexibility and discrete heterogeneity from single particle cryo-EM. *J. Struct. Biol.* **213**, 107702 https://doi.org/10.1016/j.jsb.2021.107702
92 Zhang, K., Julius, D. and Cheng, Y. (2021) Structural snapshots of TRPV1 reveal mechanism of polymodal functionality. *Cell* **184**, 5138–5150.e12 https://doi.org/10.1016/j.cell.2021.08.012
93 Maeots, M.E., Lee, B., Nans, A., Jeong, S.G., Esfahani, M.M.N., Ding, S. et al. (2020) Modular microfluidics enables kinetic insight from time-resolved cryo-EM. *Nat. Commun.* **11**, 3465 https://doi.org/10.1038/s41467-020-17230-4
94 Dandey, V.P., Budell, W.C., Wei, H., Bobe, D., Maruthi, K., Kopylov, M. et al. (2020) Time-resolved cryo-EM using Spotiton. *Nat. Methods* **17**, 897–900 https://doi.org/10.1038/s41592-020-0925-6
95 Kawai, T., Sun, B., Yoshino, H., Feng, D., Suzuki, Y., Fukazawa, M. et al. (2020) Structural basis for GLP-1 receptor activation by LY3502970, an orally active nonpeptide agonist. *Proc. Natl Acad. Sci. U.S.A.* **117**, 29959–29967 https://doi.org/10.1073/pnas.2014879117